Modeling the original and cyclic compression behavior of non-woven gas diffusion layers for fuel cells

Christophe Carral, Patrice Mele

Modeling the original and cyclic compression behavior of non-woven gas diffusion layers for fuel cells

Christophe Carral[1] and Patrice Mele[1]

[1] *Univ. Grenoble Alpes, Univ. Savoie Mont Blanc, CNRS, Grenoble INP, LEPMI, 38000 Grenoble, France*

International Journal of Hydrogen Energy, 47, 23348-23359, 2022
https://doi.org/10.1016/j.ijhydene.2022.05.121

Abstract

It is established that the compression behavior of gas diffusion layers (GDL) is dependent on the level of the mechanical stress it experienced during its lifetime. As a matter of fact, every cycle of compression induces damages in the GDL, including fibers breakage and/or their spatial reorganization. As observed in the experimental work, the first cycle of compression of GDLs as received from the suppliers is already altered by a previous compression that is applied during the manufacturing process. This paper then presents a model able to predict the cyclic behavior of GDL, considering the existence of this compressive stress applied during the manufacturing process. The experimental mechanical properties of the three main types of non-woven GDL (rolls, sheets and felts) were first measured and then predicted using the proposed model, thereby allowing to separate the influences of the manufacturing process, the type of fibers, the presence of a micro-porous layer and a hydrophobic treatment on the GDL.

Keywords— Proton exchange membrane fuel cell, Gas diffusion layer, Non-linear mechanical behavior, Compression, Constitutive model

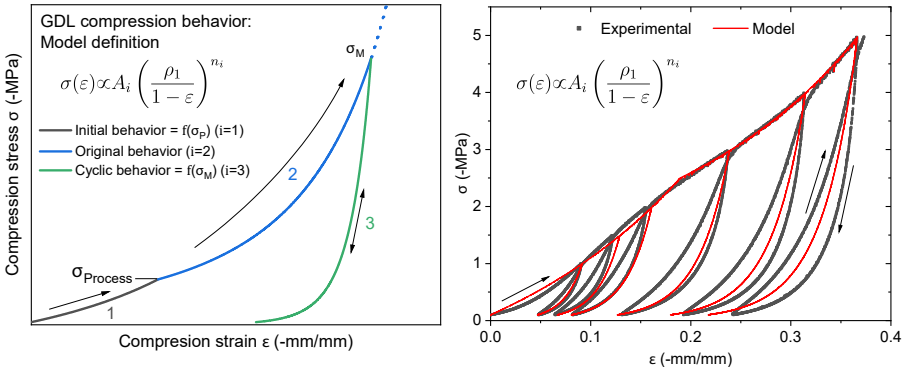

Graphical Abstract

1 Introduction

Mechanics is recently becoming a center of interest in the research for performance and durability of proton exchange membrane fuel cells (PEMFCs), which is proven by the numerous studies and reviews on the subject [1–5]. It is indeed shown in different experimental studies [6–16] that the performance of PEMFCs require the control of the mechanical state of the stack, and especially of the gas diffusion layer (GDL) [15–19].

The GDL is a porous media, composed of carbon fibers, located between the flow field of the bipolar plates (BPPs) and the catalyst layers (CLs). Different types of GDL are used in PEMFCs, including non-woven carbon paper and woven carbon cloth [18, 20, 21]. In the non-woven category, the final product can be presented in three forms: sheets, rolls or felts. Sheets and rolls are composed of straight carbon fibers, whereas felts are composed of curved carbon fibers. Sheets present higher in-plane Young's moduli, in the range of 5 to 10 GPa [22–24], compare to the one of rolls or felts, whose values are between 1 and 3 GPa [23, 24]. The higher in-plane stiffness of sheets results to additional graphitization step in the process that is not present in the manufacturing of rolls [20]. Furthermore, the low in-plane stiffness of felts is related to the curvature of the fibers.

The GDL plays an essential role in the operation of a PEMFC; its various functions are (i) to diffuse uniformly the reactant gases on the active layers, (ii) to provide an electrical and thermal connection, thereby conducting electrons and heat between the CLs and towards the BPPs and (iii) to participate in the elimination of the water produced by the electrochemical reactions. All these essential functions can be affected by the mechanical state of the GDL. For example, Chang et al. [8] showed that increasing the GDL compression decreases its porosity rate thereby reducing the gas diffusion path. Conversely, it will improve the GDL electrical and thermal conductivity, as well as its contact resistance with the BPP and CL [25–27]. Recent studies [28–32] have demonstrated that the water management is strongly affected by the GDL compression, mostly in the mass transport region.

It is therefore necessary to know and understand the mechanical behavior of the GDL, especially during its compression. Being a porous media, GDLs exhibit an original behavior in compression as characterized by a strong non-linearity and a dependency on the level of compression that is applied on the samples [20, 23, 33–46]. New contacts are created between the fibers during the GDL compression, thus increasing its stiffness [36, 39, 44]. Fiber breakage can also occur, leading to residual deformations and a different behavior [20, 37, 39, 40, 43–45]. In this way, it is difficult to define a model allowing to predict with precision the compression behavior of GDLs. Polynomial fits have been proposed by different authors [35, 38, 47, 48] to model the initial non-linear compression. Different models based on the beam theory, in the hypothesis that the fibers composing the GDL bend between contact points, have been proposed by different authors [36, 39, 49, 50]. The latter model exhibits a good prediction of the GDL experimental behavior, but is applicable only for stress value lower than the maximum compression pressure experienced by the GDL. Shi et al. enhanced the model of Gigos by implementing the Hertz contact effect. Carral and Mele [44] showed that the compression of GDL can be predicted by the physical model developed by Van-Wyk and Toll [51, 52] for the compression of fibrous materials, bringing a new proof that the compression behavior of GDLs is directly linked to the number of contact points between fibers. Poornesh and Bhat [53, 54] proposed a phenomenological model to describe the cyclic response of GDLs. Meng et al. [45] developed recently a non-linear constitutive model which described the cyclic compression of felts GDL accurately. This last model is based on the observation that the tangent modulus of the felts GDL compression follows a linear increase with the compression stress.

The initial behavior of GDLs can be however affected by the compression pressure ap-

plied during the manufacturing process, as we observed in the experimental work proposed in this article. The previous models are not able to take in account of this phenomenon. A new improved model is thus proposed in this article, which is capable of predicting the initial and cyclic behavior of GDLs, thereby integrating their history using the definition of compression applied during the manufacturing process. The three main types of non-woven GDLs used in PEMFCs (rolls, papers and felts), exhibiting different manufacturing process, will be considered. The influence of the hydrophobic treatment and the presence of a micro-porous layer will be included as well in this study. The objective is to propose a model capable of predicting mechanical behavior of the GDL that is loaded in cyclic compression, and then taking into account its previous mechanical history. The small differences observed between experimental and predicted data, lower than 5% for all suppliers and references, prove the accuracy of the proposed model and its wilder field of application.

2 Materials and methods

2.1 GDL Samples

Four different GDL references were used in this study (Table 1) to confirm the relevance of the model and reveal the influence of their prior manufacturing process:

- Rolls, represented by refs. 36AA and 36BB, are composed of straight carbon fibers. Their low in-plane Young's modulus (≈1-3 GPa [23]) allows the manufacturers to produce them as a continuous roll good. Ref. 36BB will allow to analyze the influence of micro-porous layer (MPL) and hydrophobic treatment.
- Sheets, represented by ref. H060, are composed of straight graphite fibers. They exhibit a high in-plane Young's modulus (≈10 GPa [23]), mainly due to the additional graphitization step in the manufacturing process [20]. Therefore, they cannot be rolled and are commercialized in a sheet form.
- Felts, represented by ref. H23C7, are composed of curved carbon fibers. They exhibit a low in-plane modulus and can be produced as continuous roll good.

Supplier	Reference	Areal weight $g.m^2$	Thickness [a] μm	Bulk density [a] $g.cm^{-3}$	Type
SGL	36AA	57±3	221±3	0.26±0.01	Roll
SGL	36BB	103±3	267±2	0.39±0.01	Roll with MPL
Toray	H060	86±2	193±3	0.45±0.02	Sheet
Freundenberg	H23C7	134±2	230±7	0.59±0.02	Felt with MPL

[a] @0.1 MPa

Table 1: References and technical data of the GDL samples (variability is range of measurements).

.

2.2 Compression tests

The protocol detailed in [44] was used to perform the compression tests, i.e. the compression of a stack of six GDL samples of 16 mm diameter with intermediate layers composed of aluminum foils. A pressure of 0.1 MPa was taken into account to detect the contact with the samples. During the fuel cell operation, and in particular during start-up and

shutdown phases, hygrothermal cycles lead to cyclic compression of the GDLs through thermal expansion of the stack components and swelling of the membrane. To analyze the cyclic behavior of the GDLs, a series of compression cycles between the contact pressure of 0.1 MPa and different levels of compression (1-1.5-2-3-4-5 MPa) was applied on the samples, as depicted in Fig. 1.

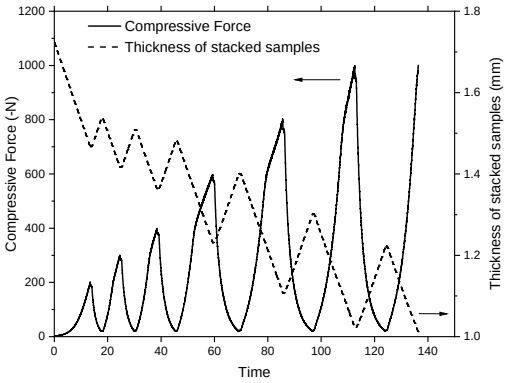

Figure 1: Compression cycles applied during the experimental tests to analyze the cyclic behavior of GDLs (example on ref. 36BB). The different force levels correspond to compressive stresses from 0.1 MPa to 1-1.5-2-3-4-5 MPa.

2.3 Graphic representation of results

2.3.1 Stress-strain curves

Stress-strain curves are the typical representation of compression tests in material science, and are used in most of existing GDLs mechanical studies [20, 23, 33–43]. It allows the application of continuum mechanics and their implementation into numerical simulations such as finite element analysis.

In this representation, the engineering stress σ and strain ε are calculated as follow:

$$\sigma = \frac{F}{A_0} \tag{1}$$

$$\varepsilon = \frac{\Delta_L}{t_1} \tag{2}$$

with F the compression force, A_0 the initial sample area, Δ_L the displacement of the upper compression plate and t_1 the initial thickness of the GDL samples stacked. The latter is estimated via the measurement of the thickness at the first compression under the contact pressure $\sigma_c = 0.1$ MPa.

2.3.2 Stress-relative density curves

Another representation is often employed in the case of compression of fibrous materials [51, 55–58], involves the plotting of the stress versus the relative density of the sample ρ. This representation has notably been used in the Van-Wyk Toll model showing that the compression of fibrous material is directly linked to its relative density (cf. next section). The relative density ρ is an intrinsic parameter, by contrast of the strain which is relative to the initial thickness of the sample. It can be evaluated via the following expression:

$$\rho(t) = \frac{A_w}{\rho_f t} \tag{3}$$

with A_w the areal weight of the GDL sample, ρ_f the fiber density and t the thickness of the samples during the compression. The fiber density will be assumed to be equal to 1.8 g.cm^{-3} [20, 44].

2.4 Van Wyk-Toll model

Van Wyk [51] and Toll [52, 59] analyzed the statistical distribution of fiber-fiber contact points as a function of the fibers orientation and morphological properties. Their works showed that the number of contact points between the fibers follows a power law in function of the relative density. Based on these elements and the bending theory, they developed a model capable of predicting the compression behavior of fibrous material as follow:

$$\sigma(\rho) = AE(\rho^n - \rho_c^n) \tag{4}$$

with A a dimensionless constant, E the fibers tensile modulus and n an exponent related to the fibers orientation. ρ_c is the value of the relative density for which the material exhibits a mechanical response.

In a previous work [44], it has been showed that this model can also be used to fit the compression curves of gas diffusion layers. Combining Eqn. 2, 3 and 4, it is then possible to link the mechanical compression stress directly to the strain via the following relation:

$$\sigma(\varepsilon) \propto A_i \left(\frac{\rho_1}{1-\varepsilon} \right)^{n_i} \tag{5}$$

with ρ_1 the relative density of the sample as received from the suppliers.

The latter relation will be employed to predict the variation of the experimental data of the different GDLs gathered during the compression tests. The subscript i will correspond to the different parts of the model.

3 Experimental results

Taking into account the previous remarks, the stress-strain curves of the different GDLs will be plotted as well as the stress-relative density curves for all experimental tests.

3.1 Initial behavior after manufacturing process

The initial behavior of the GDLs, that is the properties in compression of the samples as received from the supplier, is investigated in a first step. The experimental stress-strain and stress-relative density curves are depicted on Figure 2 (a) and (b). As already observed in previous works [20, 23, 33–45], a non-linear behavior of the GDLs can be observed in Figure 2 (a), characterized by a strong increase of the stiffness during the compression of the samples related in the literature to the increase of the number of contact points between fibers. Felts show a singular behavior with a significantly higher stiffness. On the stress-relative density curves (Figure 2 (b)), we can observe a similar behavior for rolls and sheets for stress values above 2 MPa. There is a shift of the curves toward higher relative densities for the sheets, mainly due to a lower initial porosity. The derivatives of the curves, representative of the tangent modulus in term of strain ($d\sigma/d\varepsilon$) or relative density ($d\sigma/d\rho$) (Figure 3 (a) and (b)), confirm the similar behavior of rolls and sheets, and the discrepancy of the felts behavior. All modulus increases

in a linear way with the compression stress, as already observed by Meng et al. [45]. However, before reaching this linear regime, the tangent modulus of sheets and rolls exhibits a peak in the curves. This peak is assumed to be related to a previous mechanical compression applied before to these tests. To prove this assumption, compression tests were performed on samples previously subjected to a maximum compressive pressure $\sigma_M = 5$ MPa (lighter-colored curves in Figure 3). A peak related to this pre-stress is clearly visible in Figure 3 (a) and (b), confirming the previous hypothesis. For stress values above 5 MPa, it can be noted that all samples show similar behavior. This is confirmed on the curves presenting the derivatives of the stress/relative density curves (Figure 3 (b)), showing that this representation is independent of the previous mechanical history undergone by the samples, in contrast to the derivative of the stress/strain curves (Figure 3 (a)).

In conclusion, the inflection point observed on the derivative curves after the peak reveals the mechanical pressure applied in the past of the samples. The peak shown on the initial compression on the samples received from the suppliers can be then linked to a compression applied during the manufacturing process of the GDLs. The value of this compression, σ_P, has been then determined from the inflection points represented on the derivatives of the curves of pristine samples (zooms in Figure 3) and are gathered in Table 2.

Short Ref.	σ_P (MPa)
36AA	1.5
36BB	2.5
H060	3.2
H23C7	$\leqslant$0.5

Table 2: Estimated compression pressure applied during the manufacturing process, σ_P, of the different GDLs.

3.2 Cyclic behavior

As described in the materials and methods section, each reference was subjected to a series of compression cycles between the contact pressure of 0.1 MPa and different levels of compression (1-1.5-2-3-4-5 MPa). The maximum pressure value experienced by the

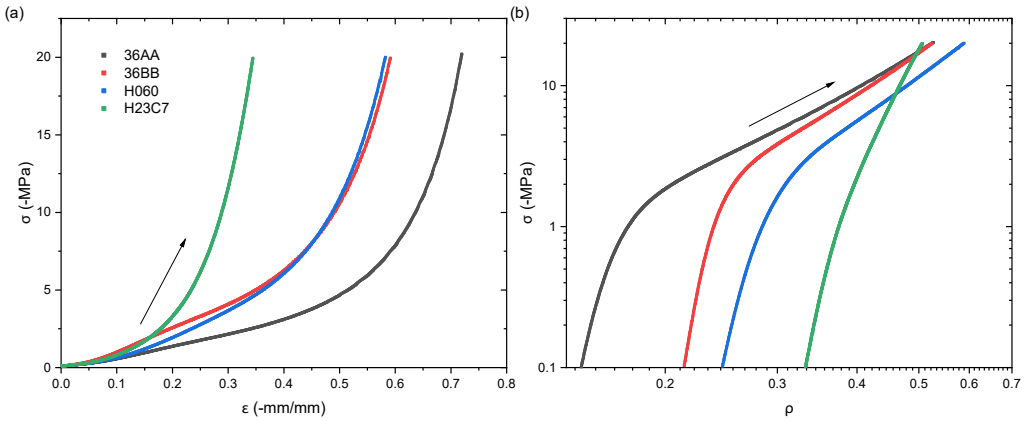

Figure 2: Experimental measurements of GDLs compression of samples as received from the supplier (pristine samples). (a) stress versus strain (linear scales) and (b) stress versus relative density (logarithmic scales).

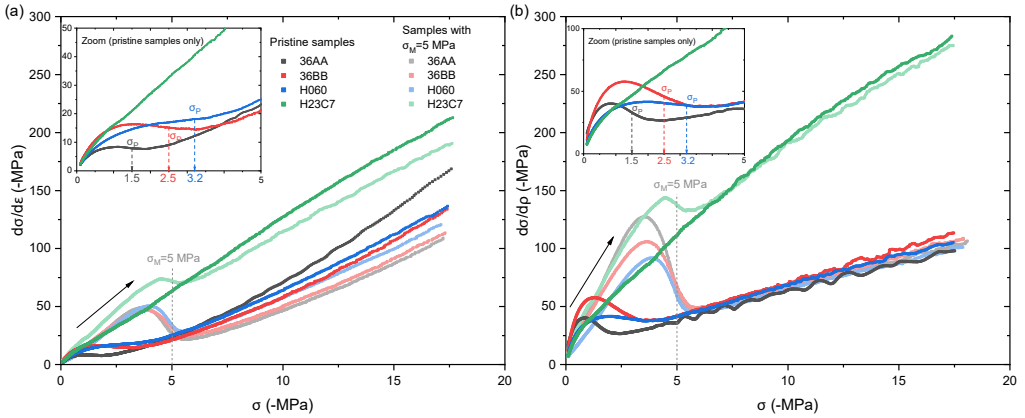

Figure 3: Derivatives of the compression curves (a) $d\sigma/d\varepsilon$ (stress/strain tangent modulus) versus stress and (b) $d\sigma/d\rho$ (stress/relative density tangent modulus) versus stress. Two sets of samples are employed: pristine samples (curves obtained in Figure 2) and samples subjected before experiment to a compression pressure $\sigma_M = 5$ MPa.

samples will be refer as σ_M. The results of the experiments are depicted in Figure 4. After each loading, the compression curves is altered for pressure values below σ_M. During the loading part of the compression, once the value of σ_M is reached, the initial behavior of the pristine sample is recovered. An hysteresis is observed between the unloading and the loading part of the compression. Roll GDLs show greater variation in behavior after mechanical cycling, in contrast to sheet and felt GDLs which exhibit better dimensional stability. This mechanical stability would be of interest to guarantee that the optimal mechanical state of the GDL is kept during the hygrothermal cycles induced by the fuel cell operation.

4 Compression model

4.1 Model description

The model explicited in section 2.4 will be employed to predict the cyclic compression of the different GDLs. It will be divided in three parts (Figure 5), according to the different behaviors exhibited in the precedent sections, and detailed thereafter.

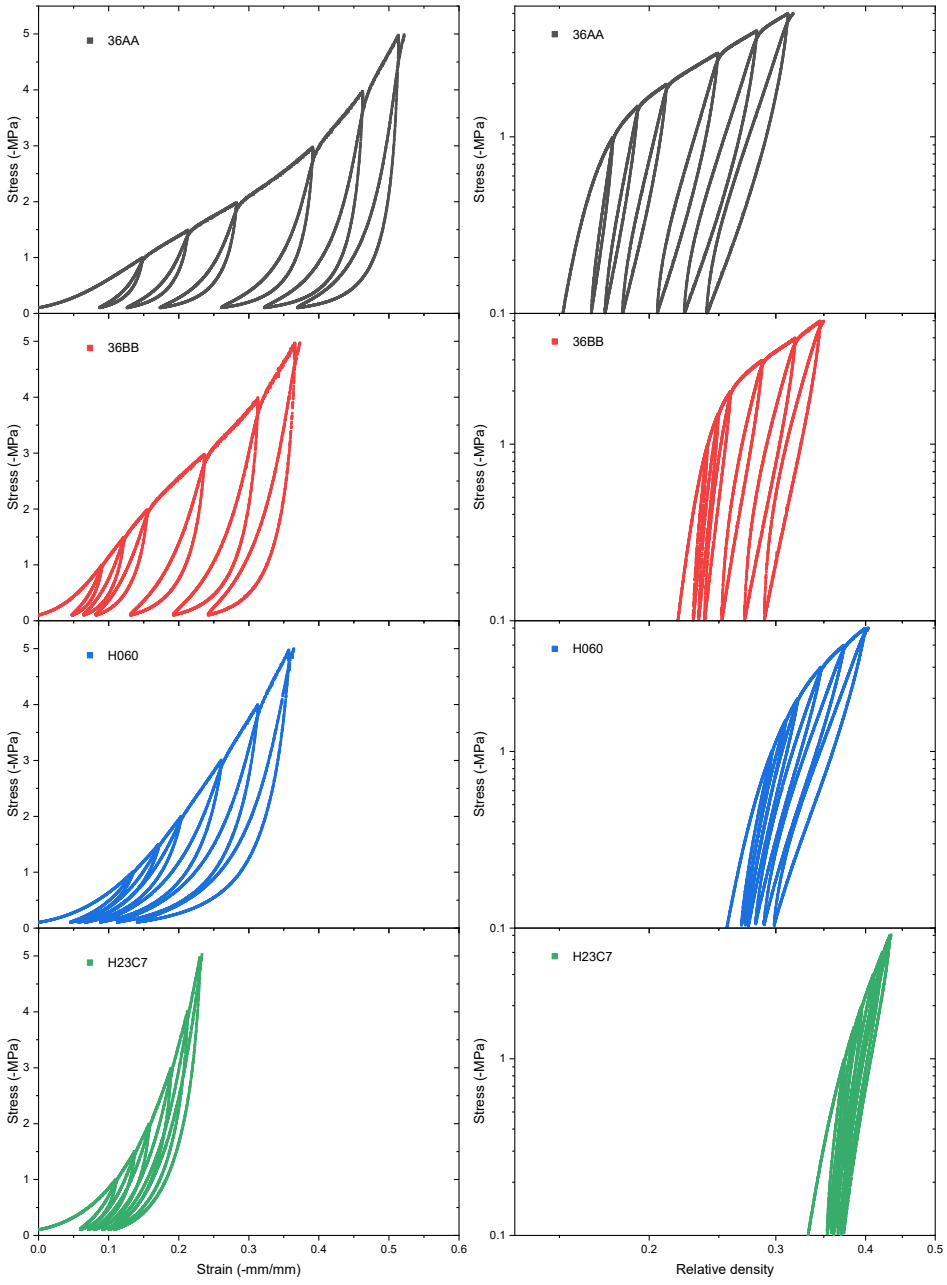

Figure 4: Cyclic compression of each GDL reference. On the left: stress-strain curves (linear scales). On the right: stress-relative density curves (logarithmic scales).

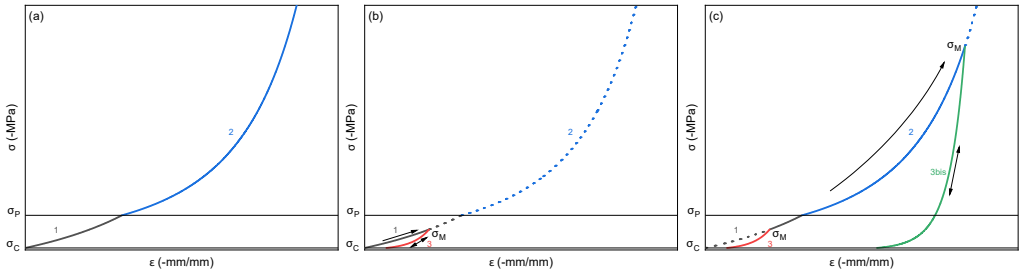

Figure 5: Graphical illustration of the model divided in 3 parts: (a) initial compression of the GDL with the damaged behavior after manufacturing (curve 1) and the original behavior (curve 2), separated by σ_P, (b) compression cycling to a stress level $\sigma_M < \sigma_P$ inducing residual deformation and the new behavior (curve 3), (c) compression cycling to a higher stress level $\sigma_M > \sigma_P$ inducing residual deformation and a new behavior (curve 3bis). σ_P corresponds to the pressure applied during the manufacturing process and σ_c corresponds to the contact pressure applied to detect the contact with the samples.

1-Initial behavior after manufacturing ($\sigma \leqslant \sigma_P$): This first part of the model will be related to the manufacturing process. The compression loading for pressure below σ_P can be determined by the following relation (Eqn. 6):

$$\sigma_1 = A_1 \left(\left(\frac{\rho_1}{1-\varepsilon} \right)^{n_1} - \rho_1^{n_1} \right) + \sigma_c \tag{6}$$

2-original behavior ($\sigma \geqslant \sigma_P$): during the compression loading, once the value of σ_P is reached, the original behavior of the GDL is recovered (Figure 5 a, curve 2). This behavior depends on the fibers properties (diameter, length, shape (straight or curved), their stiffness (graphitized or not) and their spatial distribution, including their number of contacts and its evolution with the deformation. This behavior can be described by the following equation (Eqn. 7):

$$\sigma_2 = A_2 \left(\frac{\rho_1}{1-\varepsilon} \right)^{n_2} \tag{7}$$

3-4 cyclic behavior ($\sigma \leqslant \sigma_M$): if any compression was already applied to the GDLs, the compression path will be modified accordingly. The loading and unloading will follow a same path, hence the hysteresis of the compression cycle will not be taken into account. This new behavior, depending of the level of σ_M applied, is the results of the damages incurred by the GDL during previous compression, including fibers breakage and their reorganization. Eqn. (8) below will define this damaged behavior, with parameters depending on the value of σ_M.

$$\sigma_3 = A_3 \left(\frac{\rho_1}{1-\varepsilon} \right)^{n_3} \tag{8}$$

4.2 Methodology to obtain the different parameters

In the previous equations, 8 parameters are needed to predict the initial, original, and cyclic behavior of the GDLs. This section is devoted to the description of their determination. The GDL 36BB will be taken as example to show this methodology. All parameters will be obtained from the test described in Figure 4.

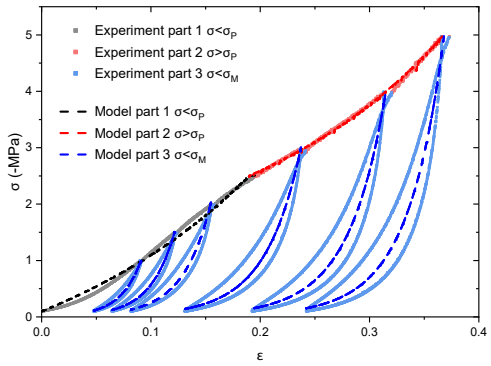

Figure 6: Model definition via the experimental measurements shown in Figure 4. Example on ref. 36BB.

4.2.1 GDL behavior after the manufacturing process: determination of the parameters A_1, n_1, ρ_1, σ_P

σ_P is depending of the manufacturing process, and can be estimated via the plot of the tangent modulus in function of the applied compressive stress (cf. Section3.1.)

ρ_1 is the initial relative density measured at σ_c. It can be determined from the initial thickness of the GDL t_1 measured at σ_c and the following relationship (Eqn. 9):

$$\rho_1 = \frac{A_w}{\rho_f t_1} \tag{9}$$

The parameters A_1 and n_1 are obtained by fitting the experimental measurements above σ_M and below σ_P from Eqn. (6) as shown in Figure 6 (part 1).

4.2.2 GDL original behavior: determination of the parameter n_2

The parameter n_2 can be obtained by fitting the experimental measurements above σ_M and σ_P using Eqn. (7) as depicted in Figure 6 (part 2).

4.2.3 GDL behavior after cycling compression: determination of the parameter n_3

The GDL behavior after cycling compression is dependent of the stress σ_M, i.e. the maximum stress experienced during the compression cycles.

Different values of n_3 can be obtained via the fitting of the experimental measurements below σ_M using Eqn. (8) and as depicted in Figure 6 (part 3). The final value of n_3 depending of σ_M can be evaluated via the following empirical relation:

$$n_3 = B \exp\left(\frac{-\sigma_M}{C}\right) + n_{3_0} \tag{10}$$

with B, C and n_{3_0} the fitting parameters obtained as depicted in Figure 7. n_{3_0} corresponds to the asymptotic value of n_3 for infinite values of σ_M.

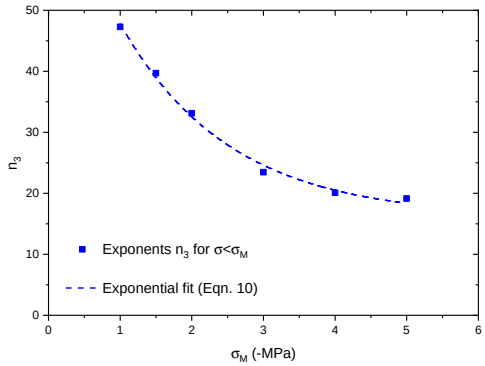

Figure 7: Fitting of the evolution of the exponent n_3 with σ_M. Example on ref. 36BB.

4.2.4 Calculated parameters: A_2, A_3

The other parameters can be then calculated by assuming the continuity of the model between the parts and the following expressions:

$$A_2 = \frac{\sigma_P}{(\frac{\sigma_P - \sigma_c}{A_1} + \rho_1^{n_1})^{n_2/n_1}} \tag{11}$$

$$For\ \sigma_M \leqslant \sigma_P : A_3 = \frac{\sigma_M}{(\frac{\sigma_M - \sigma_c}{A_1} + \rho_1^{n_1})^{n_3/n_1}} \tag{12}$$

$$For\ \sigma_M \geqslant \sigma_P : A_3 = \frac{\sigma_M}{(\frac{\sigma_M}{A_2})^{n_3/n_2}} \tag{13}$$

4.3 Comparison of the model versus experimental measurements

A comparison of the experimental and predicted results using the model described in this article is shown in Figure 8 for the 4 GDLs studied. All the parameters determined to predict the non-linear mechanical behavior of these GDLs are gathered in Table 3. A very good agreement between experimental and predicted data can be observed. To confirm this statement, two criteria are employed, based on the difference of strains with its absolute error $\Delta\varepsilon$ and its relative error $\Delta\varepsilon/\varepsilon$ (Table 4). It can be seen that the maximum errors during the compression cycles, going up to 0.026 mm/mm or 19% in absolute and relative strain respectively, are occuring for low compression pressures. It could be due to the fact that the hysteresis during the loading and unloading cycles is not taken into account in the proposed approach. However, in average, the errors are below 0.008 mm/mm and 3.9%, which is a successful outcome.

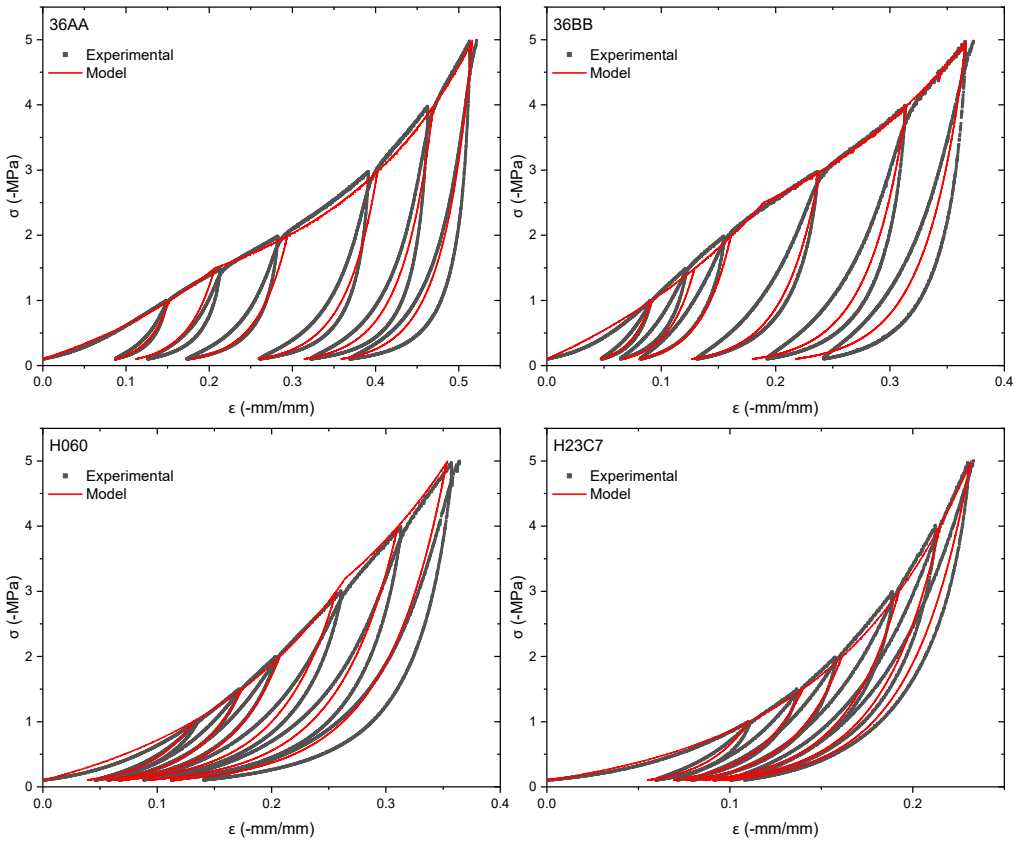

Figure 8: Comparison of the cyclic stress/strain curves obtained with the model and the experimental measurements.

Short Ref.	σ_P MPa	ρ_1	A_1 MPa	n_1	n_2	B	C	n_{3_0}
36AA	1.5	0.152	298.7	2.81	2.43	50.0	0.95	13.6
36BB	2.5	0.219	341.7	3.25	2.79	61.2	1.52	16.1
H060	3.2	0.257	549.1	4.67	3.44	19.4	2.03	10.6
H23C7	0	0.332	14150	9.39	9.39	27.8	1.64	22.6

Table 3: Model parameters, for a contact pressure σ_c=0.1 MPa.

Short Ref.	Absolute error ($\Delta\varepsilon$)	Relative error ($\Delta\varepsilon/\varepsilon$)
36AA	0.008 (0.024)	2.6% (9.7%)
36BB	0.007 (0.022)	3.9% (19%)
H060	0.008 (0.026)	3.6% (16%)
H23C7	0.005 (0.016)	3.5% (12%)

Table 4: Values of the absolute ($\Delta\varepsilon$) and relative error ($\Delta\varepsilon/\varepsilon$) between experimental and predicted data. (Average value on all compression cycles, the number in bracket is the maximum value encountered during the compression cycles).

5 Conclusion

The experimental part of this work sheds light on the influence of the manufacturing process on the mechanical behavior of gas diffusion layers. A prior compression has been revealed on the samples as received from the suppliers, which affects the behavior of the first cycle of compression. The existing models developed to predict the GDLs mechanical behavior do not take into account this phenomenon. Therefore, a non-linear model for the compression of non-woven gas diffusion layers, able to capture the effect of the pressure applied during the manufacturing process, is proposed. This new model offers the possibility to simulate the cyclic compression of the GDLs integrating the initial behavior of the GDL, the original behavior of the GDL without any compression experienced, and the new behavior after compression cycles. The model is then divided into three parts relative to these different behaviors. A set of 8 given parameters is sufficient for the complete definition of the model. The three main types of non-woven GDL (roll, sheet, felt) have been employed to analyze the influence of the manufacturing process, the fibers type, the presence of a micro-porous layer and hydrophobic treatment on the GDL. It has been observed that all GDLs with straight fibers (rolls and sheets) have similar original mechanical behavior. GDLs with curved fibers (felts) are significantly stiffer in compression compare to the rolls A better dimensional stability during compression cycles is observed for the sheets and the felts, which is likely due to the graphitization step during the process of sheets and the organization of the curved fibers for the felts. A good agreement is obtained between experimental and predicted data, the errors in strains being below 0.008 mm/mm and 3.9% in average for all types of GDL employed in this study.

This model can be now implemented in numerical simulations to analyze the influence of cycles of stresses and strains induced by the fuel cell operation on the GDLs and its effects on the membrane and active layers. This will be the aim of a future work.

Acknowledgments

This work has been partially funded by the CNRS Energy unit (Cellule Energie) through the project DEVOPEM, and by the CARNOT project OPTIPEM. The authors are grateful to SGL Carbon Company, especially Susanne Bacher and Nico Haak, for providing SGL GDL samples.

Annexes: Addendum to the model

5.1 Prediction of the compression behavior in function of the GDL porosity ϕ

If the material would be composed of fibers exclusively, the relative density ρ would be equal to the fibers volume fraction. The void fraction ϕ, i.e. the porosity of the GDL, could be then calculated with the following expression:

$$\phi = 1 - \rho \tag{14}$$

It is then possible to directly link the compressive stress to one of the main function of the GDL, which is the gas permeability via its porosity:

$$\sigma_1 = A_1((1-\phi)^{n_1} - (1-\phi_1)^{n_1}) + \sigma_c \tag{15}$$

$$\sigma_2 = A_2(1-\phi)^{n_2} \tag{16}$$

$$\sigma_3 = A_3(1-\phi)^{n_3} \tag{17}$$

with ϕ_1 the initial porosity of the GDL

5.2 Calculation of the GDL residual strain

The following equation is available to calculate the residual strain ε_R after applying a given value of stress σ_M. The parameters A_3 and n_3 must be updated previously according to the level of stress σ_M reached (cf. Eqn. 10, 12 and 13).

$$\varepsilon_R = 1 - \rho_1 \left(\frac{A_3}{\sigma_c}\right)^{1/n_3} ; \tag{18}$$

5.3 Calculation of the tangent modulus

The following equations are available to calculate the tangent modulus E_T from the model parameters.

$$E_{T_i} = A_i \rho_1 n_i \left(\frac{\rho_1}{(\varepsilon-1)}\right)^{n_i-1} (\varepsilon-1)^{-2} \tag{19}$$

with i=1 to 3 according to the level of σ and σ_M reached during the GDL compression (cf. Section 4).

5.4 Calculation of the strain in function of the stress

The following equations are available to calculate the reciprocal of the model i.e. the strain in function of the stress:

$$\varepsilon_1 = 1 - \rho_1 \left(\frac{A_1}{(\sigma - \sigma_c + \rho_1^{n_1} A_1}\right)^{1/n_1} \tag{20}$$

$$\varepsilon_2 = 1 - \rho_1 \left(\frac{A_2}{\sigma}\right)^{1/n_2} \tag{21}$$

$$\varepsilon_3 = 1 - \rho_1 \left(\frac{A_3}{\sigma}\right)^{1/n_3} \tag{22}$$

Nomenclature

A_0 the initial sample area

A_i a dimensionless constant

A_w the areal weight

B a dimensionless constant

C a dimensionless constant

E the Young's modulus

E_t the tangent Young's modulus

F the force

i subscript corresponding the different parts of the compression model

n_i a dimensionless constant

n_{30} a dimensionless constant

t the thickness

t_1 the initial thickness

Δ_L the displacement measured during the compression test

ε the mechanical strain

ε_R the residual strain

ϕ the GDL porosity

ϕ the initial GDL porosity

ρ the relative density

ρ_1 the initial GDL relative density

ρ_f the fiber density

ρ_c the critical density

σ the mechanical stress

σ_P the compression pressure applied during the GDL manufacturing process

σ_C the compression pressure value to detect the contact with the samples during the tests

σ_M the maximum mechanical stress experienced by the GDL during compression cycles

References

[1] Wei Zhang and Cheng-wei Wu. Effect of clamping load on the performance of proton exchange membrane fuel cell stack and its optimization design: a review of modeling and experimental research. *Journal of fuel cell science and technology*, 11(2), 2014.

[2] Jason Millichamp, Thomas J Mason, Tobias P Neville, Natarajan Rajalakshmi, Rhodri Jervis, Paul R Shearing, and Daniel JL Brett. Mechanisms and effects of mechanical compression and dimensional change in polymer electrolyte fuel cells–a review. *J. Power Sources*, 284:305–320, 2015.

[3] Ahmed Mohmed Dafalla and Fangming Jiang. Stresses and their impacts on proton exchange membrane fuel cells: A review. *Int. J. Hydrogen Energ.*, 43:2327–2348, 2017.

[4] Khadidja Bouziane, Nada Zamel, Xavier Francois, Yann Meyer, Denis Candusso, et al. Effects of mechanical compression on the performance of polymer electrolyte fuel cells and analysis through in-situ characterisation techniques-a review. *J. Power Sources*, 424:8–26, 2019.

[5] GR Molaeimanesh and M Nazemian. Investigation of gdl compression effects on the performance of a pem fuel cell cathode by lattice boltzmann method. *J. Power Sources*, 359:494–506, 2017.

[6] Woo-Kum Lee, Chien-Hsien Ho, J. W. Van Zee, and Mahesh Murthy. The effects of compression and gas diffusion layers on the performance of a PEM fuel cell. *J. Power Sources*, 84(1):45–51, 1999.

[7] Jiabin Ge, Andrew Higier, and Hongtan Liu. Effect of gas diffusion layer compression on PEM fuel cell performance. *J. Power Sources*, 159(2):922–927, 2006.

[8] W.R. Chang, J.J. Hwang, F.B. Weng, and S.H. Chan. Effect of clamping pressure on the performance of a PEM fuel cell. *J. Power Sources*, 166(1):149–154, 2007.

[9] Xinting Wang, Ying Song, and Bi Zhang. Experimental study on clamping pressure distribution in PEM fuel cells. *J. Power Sources*, 179(1):305–309, 2008.

[10] Chih-Yung Wen, Yu-Sheng Lin, and Chien-Heng Lu. Experimental study of clamping effects on the performances of a single proton exchange membrane fuel cell and a 10-cell stack. *J. Power Sources*, 192(2):475–485, 2009.

[11] Sung-Dae Yim, Byung-Ju Kim, Young-Jun Sohn, Young-Gi Yoon, Gu-Gon Park, Won-Yong Lee, Chang-Soo Kim, and Yong Chai Kim. The influence of stack clamping pressure on the performance of PEM fuel cell stack. *Curr. Appl Phys.*, 10(2, Supplement 1):S59–S61, 2010.

[12] C.-Y. Wen, H.-T. Chang, and T.-W. Luo. Simulation methodology on analyzing clamping mode for single proton exchange membrane fuel cell. *J. Mech.*, 27:545–558, 2011.

[13] Hao-Ming Chang, Chien-Wei Lin, Min-Hsing Chang, Huan-Ruei Shiu, Wen-Chen Chang, and Fang-Hei Tsau. Optimization of polytetrafluoroethylene content in cathode gas diffusion layer by the evaluation of compression effect on the performance of a proton exchange membrane fuel cell. *J. Power Sources*, 196(8):3773–3780, 2011.

[14] Thomas J. Mason, Jason Millichamp, Tobias P. Neville, Paul R. Shearing, Stefaan Simons, and Daniel J.L. Brett. A study of the effect of water management and electrode flooding on the dimensional change of polymer electrolyte fuel cells. *J. Power Sources*, 242(0):70–77, 2013.

[15] RW Atkinson, Yannick Garsany, Benjamin D Gould, Karen E Swider-Lyons, and Iryna V Zenyuk. The role of compressive stress on gas diffusion media morphology and fuel cell performance. *ACS Applied Energy Materials*, 1(1):191–201, 2017.

[16] Philipp Irmscher, D Qui, Holger Janßen, Werner Lehnert, and Detlef Stolten. Impact of gas diffusion layer mechanics on pem fuel cell performance. *Int. J. Hydrogen Energy*, 44(41):23406–23415, 2019.

[17] Xiaohui Yan, Chen Lin, Zhifeng Zheng, Junren Chen, Guanghua Wei, and Junliang Zhang. Effect of clamping pressure on liquid-cooled pemfc stack performance considering inhomogeneous gas diffusion layer compression. *Appl. Energy*, 258:114073, 2020.

[18] Qitong Shi, Cong Feng, Pingwen Ming, Fumin Tang, and Cunman Zhang. Compressive stress and its impact on the gas diffusion layer: A review. *Int. J. Hydrogen Energy*, 2022.

[19] F Aldakheel, MS Ismail, KJ Hughes, DB Ingham, L Ma, and M Pourkashanian. Effects of compression on mechanical integrity, gas permeability and thermal stability of gas diffusion layers with/without sealing gaskets. *Int. J. Hydrogen Energy*, 46(44):22907–22919, 2021.

[20] MF Mathias, Joerg Roth, Jerry Fleming, and Werner Lehnert. Diffusion media materials and characterisation. *Handbook of fuel cells*, 2003.

[21] Sehkyu Park, Jong-Won Lee, and Branko N. Popov. A review of gas diffusion layer in PEM fuel cells: Materials and designs. *Int. J. Hydrogen Energy*, 37(7):5850–5865, apr 2012.

[22] S.R. Dhanushkodi, F. Capitanio, T. Biggs, and W. Mérida. Understanding flexural, mechanical and physico-chemical properties of gas diffusion layers for polymer membrane fuel cell and electrolyzer systems. *Int. J. Hydrogen Energy*, 40(46):16846–16859, dec 2015.

[23] J. Kleemann, F. Finsterwalder, and W. Tillmetz. Characterisation of mechanical behaviour and coupled electrical properties of polymer electrolyte membrane fuel cell gas diffusion layers. *J. Power Sources*, 190(1):92–102, 2009.

[24] Marwa Ouerghemmi, Christophe Carral, and Patrice Mele. Experimental study of gas diffusion layers nonlinear orthotropic behavior. In *E3S Web of Conferences*, volume 334, page 04020. EDP Sciences, 2022.

[25] Iwao Nitta, Tero Hottinen, Olli Himanen, and Mikko Mikkola. Inhomogeneous compression of PEMFC gas diffusion layer: Part i. experimental. *J. Power Sources*, 171(1):26–36, 2007.

[26] I. Nitta, S. Karvonen, O. Himanen, and M. Mikkola. Modelling the effect of inhomogeneous compression of GDL on local transport phenomena in a PEM fuel cell. *Fuel Cells*, 8(6):410–421, 2008.

[27] Khadidja Bouziane, Rémy Lachat, Nada Zamel, Yann Meyer, Denis Candusso, et al. Impact of cyclic mechanical compression on the electrical contact resistance between the gas diffusion layer and the bipolar plate of a polymer electrolyte membrane fuel cell. *Renewable Energy*, 153:349–361, 2020.

[28] Utku U Ince, Henning Markötter, Michael G George, Hang Liu, Nan Ge, Jongmin Lee, Saad S Alrwashdeh, Roswitha Zeis, Matthias Messerschmidt, Joachim Scholta, et al. Effects of compression on water distribution in gas diffusion layer materials of pemfc in a point injection device by means of synchrotron x-ray imaging. *Int. J. Hydrogen Energy*, 43(1):391–406, 2018.

[29] Y Wu, JIS Cho, X Lu, L Rasha, TP Neville, J Millichamp, R Ziesche, N Kardjilov, H Markötter, P Shearing, et al. Effect of compression on the water management of polymer electrolyte fuel cells: An in-operando neutron radiography study. *J. Power Sources*, 412:597–605, 2019.

[30] Nivedita Kulkarni, Jason IS Cho, Lara Rasha, Rhodri E Owen, Yunsong Wu, Ralf Ziesche, Jennifer Hack, Toby Neville, Michael Whiteley, Nikolay Kardjilov, et al. Effect of cell compression on the water dynamics of a polymer electrolyte fuel cell using in-plane and through-plane in-operando neutron radiography. *J. Power Sources*, 439:227074, 2019.

[31] Yifan Xu, Diankai Qiu, Peiyun Yi, Shuhuai Lan, and Linfa Peng. An integrated model of the water transport in nonuniform compressed gas diffusion layers for pemfc. *Int. J. Hydrogen Energy*, 44(26):13777–13785, 2019.

[32] Lijun Zhu, Heng Zhang, Liusheng Xiao, Aimy Bazylak, Xin Gao, and Pang-Chieh Sui. Pore-scale modeling of gas diffusion layers: Effects of compression on transport properties. *J. Power Sources*, 496:229822, 2021.

[33] V Mishra, F Yang, and R Pitchumani. Measurement and prediction of electrical contact resistance between gas diffusion layers and bipolar plate for applications to PEM fuel cells. *J. Fuel Cell Sci. Technol.*, 1(1):2–9, 2004.

[34] Sylvie Escribano, Jean-Francois Blachot, Jérémy Ethève, Arnaud Morin, and Renaut Mosdale. Characterization of PEMFCs gas diffusion layers properties. *J. Power Sources*, 156(1):8–13, 2006.

[35] M. S. Ismail, A. Hassanpour, D. B. Ingham, L. Ma, and M. Pourkashanian. On the compressibility of gas diffusion layers in proton exchange membrane fuel cells. *Fuel Cells*, 12(3):391–397, 2012.

[36] Vahid Norouzifard and Majid Bahrami. Deformation of PEM fuel cell gas diffusion layers under compressive loading: An analytical approach. *J. Power Sources*, 264:92–99, 2014.

[37] Vijay Radhakrishnan and Prathap Haridoss. Effect of cyclic compression on structure and properties of a gas diffusion layer used in PEM fuel cells. *Int. J. Hydrogen Energ.*, 35(20):11107–11118, 2010.

[38] Sogol Roohparvarzadeh. Experimental characterization of the compressive behaviour of gas diffusion layers in PEM fuel cells. Master's thesis, University of Waterloo, Canada, 2014.

[39] PA Gigos, Y Faydi, and Y Meyer. Mechanical characterization and analytical modeling of gas diffusion layers under cyclic compression. *Int. J. Hydrogen Energ.*, 40(17):5958–5965, 2015.

[40] Soufiane El Oualid, Rémy Lachat, Denis Candusso, and Yann Meyer. Characterization process to measure the electrical contact resistance of gas diffusion layers under mechanical static compressive loads. *Int. J. Hydrogen Energ.*, 42(37):23920–23931, 2017.

[41] Younés Faydi, Remy Lachat, Philippe Lesage, and Yann Meyer. Experimental characterization method of the gas diffusion layers compression modulus for high compressive loads and based on a dynamic mechanical analysis. *J. Fuel Cell Sci. Tech.*, 12(5):054501, 2015.

[42] Mussawar Ahmad, Robert Harrison, James Meredith, Axel Bindel, and Ben Todd. Validation of a fuel cell compression spring equivalent model using polarisation data. *Int. J. Hydrogen Energ.*, 42(12):8109–8118, 2017.

[43] Zhuo Zhang, Pu He, Yan-Jun Dai, Pu-Hang Jin, and Wen-Quan Tao. Study of the mechanical behavior of paper-type GDL in PEMFC based on microstructure morphology. *Int. J. Hydrogen Energy*, 2020.

[44] Christophe Carral and Patrice Mélé. A constitutive law to predict the compression of gas diffusion layers. *Int. J. Hydrogen Energ.*, 43(42):19721–19729, 2018.

[45] Lei Meng, Ping Zhou, Ying Yan, and Dongming Guo. Compression properties of gas diffusion layers and its constitutive model under cyclic loading. *Int. J. Hydrogen Energy*, 46(29):15965–15975, 2021.

[46] Yanqin Chen, Chao Jiang, and Chongdu Cho. An experimental investigation of three-dimensional mechanical characteristics of gas diffusion layers in proton electrolyte membrane fuel cells. *J. Solid State Electrochem.*, 23(7):2021–2030, 2019.

[47] Mustafa Fazil Serincan and Ugur Pasaogullari. Effect of gas diffusion layer anisotropy on mechanical stresses in a polymer electrolyte membrane. *J. Power Sources*, 196(3):1314 – 1320, 2011.

[48] Pablo A. Garcìa-Salaberri, Marcos Vera, and Ramón Zaera. Nonlinear orthotropic model of the inhomogeneous assembly compression of PEM fuel cell gas diffusion layers. *Int. J. Hydrogen Energ.*, 36(18):11856–11870, 2011.

[49] Vahid Norouzifard and Majid Bahrami. Analytical modeling of PEM fuel cell gas diffusion layers deformation under compression: Part 2-nonlinear behaviour region. *Ecs Transactions*, 61(11):13–23, 2014.

[50] Yang Xiao, Zhenhai Gao, Fei Gao, Tianyao Zhang, Wenhua Zhang, Ziqiao Li, Xiaoyuan Ma, and Jinxuan Qi. Improved analytical modeling and mechanical characterization of gas diffusion layers under compression load. *Energy Science & Engineering*, 8(8):2799–2807, 2020.

[51] CM Van Wyk. Note on the compressibility of wool. *J. Textile Institute*, 37(12):285–292, 1946.

[52] Staffan Toll. Packing mechanics of fiber reinforcements. *Polym. Eng. Sci.*, 38(8):1337–1350, 1998.

[53] Poornesh K Koorata and Santoshkumar D Bhat. Compressive cyclic response of pem fuel cell gas diffusion media. *Int. J. Hydrogen Energy*, 46(7):5570–5579, 2021.

[54] Poornesh K Koorata and Santoshkumar D Bhat. Thermomechanical stability and inelastic energy dissipation as durability criteria for fuel cell gas diffusion media with pre-assembly effects. *Int. J. Hydrogen Energy*, 47(2):1217–1228, 2022.

[55] Dominique Poquillon, Bernard Viguier, and Eric Andrieu. Experimental data about mechanical behaviour during compression tests for various matted fibres. *J. Mater. Sci.*, 40(22):5963–5970, 2005.

[56] Laurent Mezeix, Christophe Bouvet, Julitte Huez, and Dominique Poquillon. Mechanical behavior of entangled fibers and entangled cross-linked fibers during compression. *J. Mater. Sci.*, 44(14):3652–3661, 2009.

[57] Jean-Philippe Masse, Luc Salvo, David Rodney, Yves Bréchet, and Olivier Bouaziz. Influence of relative density on the architecture and mechanical behaviour of a steel metallic wool. *Scripta Mater.*, 54(7):1379–1383, 2006.

[58] J-P Masse and Dominique Poquillon. Mechanical behavior of entangled materials with or without cross-linked fibers. *Scripta Mater.*, 68(1):39–43, 2013.

[59] Staffan Toll. Note: On the tube model for fiber suspensions. *J. Rheol.*, 37(1):123–125, 1993.